Langmuir

Article

pubs.acs.org/Langmuir

Study of Amyloid β-Peptide (Aβ12-28-Cys) Interactions with Congo Red and β-Sheet Breaker Peptides Using Electrochemical Impedance Spectroscopy

Raheleh Partovi-Nia,[†] Samaneh Beheshti,[‡] Ziqiang Qin,[†] Himadri S. Mandal,[§] Yi-Tao Long,[∥] Hubert H. Girault,[⊥] and Heinz-Bernhard Kraatz*[,‡]

[†]Department of Chemistry, The University of Western Ontario, 1151 Richmond Street North, London, Ontario N6A 5B7, Canada

[‡]Department of Physical and Environmental Sciences, University of Toronto at Scarborough, 1265 Military Trail,Toronto, Ontario M1C 1A4, Canada

[§]Department of Chemistry, University of Pittsburgh, Chevron Science Center, 219 Parkman Avenue, Pittsburgh, Pennsylvania 15260, United States

[∥]Shanghai Key Laboratory of Functional Materials, East China University of Science and Technology, 130 Meilong Road, Shanghai, 200237, P. R. China

[⊥]Laboratoire d'Electrochimie Physique et Analytique, Ecole Polytechnique Fédérale de Lausanne, Station 6, CH-1015 Lausanne, Switzerland

Supporting Information

ABSTRACT: A surface-based approach is presented to study the interactions of Aβ12-28-Cys assembled on gold surfaces with Congo red (CR) and a β-sheet breaker (BSB) peptide. The various aspects of the peptide film have been examined using different electrochemical and surface analytical techniques. Cyclic voltammetry and electrochemical impedance spectroscopy (EIS) results using redox probes $[Fe(CN)_6]^{3-/4-}$ show that Aβ12-28-Cys on gold forms a stable and reproducible blocking film. EIS analysis shows that CR and BSB have different effects on the electrochemical properties of Aβ12-28-Cys films, presumably due to changes in the interactions between the film and CR and BSB. EIS results indicate that in the case of CR film resistance decreases significantly presumably due to better penetration of the solution-based redox probe into the film, whereas in the case of BSB, the film resistance increases. We interpret this difference to BSB being able to interact with the Aβ12-28-Cys on the surface and presumably forming a film that presents a higher resistance for electron transfer from the redox probe to the solution.

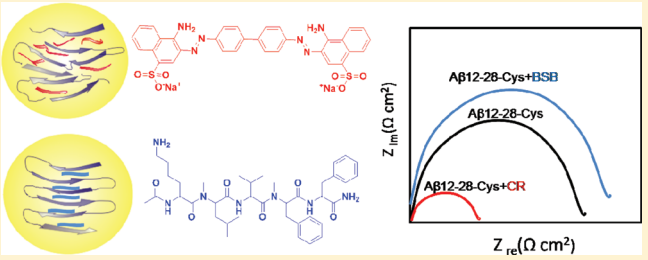

1. INTRODUCTION

Alzheimer's disease (AD) is a neurodegenerative disorder characterized by the presence of extracellular deposits of amyloid proteins and plaques in the brain, composed primarily of toxic aggregates of amyloid β-peptide (Aβ) protein.[1−3] Aβ exists in many aggregation states, ranging from dimers and trimers to fibrils and plaques, and there is increasing evidence that oligomers may be the primary pathogenic species.[4] Fibrils were initially targeted as the species responsible for neuronal toxicity and cell death. More recently, growing evidence suggests that much smaller, soluble oligomeric Aβ species correlate better with severity of AD than plaques (fibrils). Several small molecules have been reported to modulate the formation of Aβ fibrils.[4−12] For many of these compounds, the mechanisms of action are only vaguely understood. The most frequently studied of such molecules is Congo red [CR (Scheme 1a)].[13,14] However, the details of its binding mechanism and influence on protein aggregation are still not well understood.

β-Sheet breaker peptides (BSB) constitute a class of inhibitors that are designed to specifically bind Aβ peptide while preventing and reversing its conversion to a β-sheet-rich aggregated structure, precursor of the amyloid plaques.[10,15] Tjerberg and colleagues showed that Aβ16-20 is the most important region for Aβ protein−protein interaction,[16] in agreement with previous reports from several groups using Aβ mutations, which demonstrated that the central hydrophobic domain of Aβ was responsible for protein aggregation.[8,17,18] Tjerberg's studies involved the Aβ16-20 pentapeptide and demonstrated that it is able to bind to Aβ1-40 and inhibit the formation of amyloid fibrils.[16] However, Aβ16-20 spontaneously aggregates into amyloid-like fibrils, and thus, its use as an inhibitor may be problematic. Therefore, several groups have

Received: January 9, 2012
Revised: March 16, 2012
Published: March 26, 2012

Scheme 1. Molecular Structure of (a) Congo Red (CR) and of (b) a β-sheet Breaker Petide (BSB)

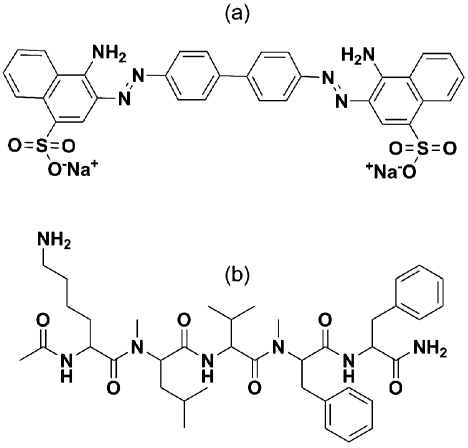

modified this sequence to produce peptide derivatives containing the self-recognition motif, along with disrupting elements that might enhance their inhibitory activity. For example, *N*-methylated peptide derivatives of Aβ16-20 have been reported that are able to bind to Aβ and disrupt its fibril formation.[19]

In the present work, we make use of C-terminal cysteine-linked Aβ12-28 (H-Val$_{12}$-His-His-Gln-Lys-Leu-Val-Phe-Phe-Ala-Glu-Asp-Val-Gly-Ser-Asn-Lys$_{28}$-Cys-OH) peptide and assemble thin films on gold in order to study the interactions with the BSB peptide Ac-Lys$_{16}$-(N-Me-Leu)-Val-(N-Me-Phe)-Phe$_{20}$-NH$_2$ (Scheme 1b) and CR using electrochemical techniques.

The 17 amino acid fragment Aβ12-28 peptide is a particularly attractive system, as it is toxic to the cell and forms amyloid fibrils similar to those found for the full-length peptide.[20] Graslund and co-workers studied the conformational properties of the Aβ12-28 peptide by using a combination of spectroscopic probes. They found a certain fraction of Aβ12-28 is in a monomeric state with a dominating random coil conformation. The monomers are in equilibrium with heterogeneous fractions of aggregates of various sizes, and these are partly in β-sheet conformation.[20,21]

Previous studies have shown that the kinetics of aggregation of Aβ is sharply dependent on peptide length.[22] In accordance with previous report,[23] aggregation of full length of Aβ (Aβ1-42 and Aβ1-43) was very fast (complete within a few minutes after dilution in phosphate buffer), whereas aggregation of Aβ12-28 was quite slow (10−30 days).[24]

Previous studies of adsorbed amyloid peptides evaluated peptide aggregation by surface plasmon resonance (SPR),[25] reflection−absorption infrared spectroscopy (RAIRS),[26] and atomic force microscopy (AFM).[27] Such an approach, while effective, does not provide control over the aggregation of the system, and in the event of strong peptide−surface attraction, a condensation of one or several condensed peptide layers at the surface becomes possible. At higher peptide concentrations, the formation of macroscopic amorphous or ordered peptide aggregates becomes possible in the bulk. In addition, conformations of peptides might be affected by the underlying surface substrate, which in turn will affect the formation of aggregates.[28,29] We want to stress that none of these studies make use of chemically modified surfaces in which an amyloid peptide is chemically attached to the surface.

In the present work, the focus is on the interaction of BSB and CR with films of the amyloid peptide fragment Aβ12-28-Cys, in which the C-terminal cysteine group allows film formation on gold surfaces. Electrochemical impedance spectroscopy (EIS) studies[30] allow us to monitor changes in impedance of the system as a function of BSB and CR addition, which can then interpreted in terms of changes in the interface and charges in the electron transfer across the modified electrode/solution interface.

2. EXPERIMETAL METHODS

2.1. Chemicals and Reagents. $K_3[Fe(CN)_6]$ and $K_4[Fe(CN)_6]$ were purchased from Aldrich. NaOH, H_2SO_4, KCl, KH_2PO4, ethanol, CR, and thioflavin T (ThT) were obtained from Sigma. Aβ12-28-Cys and BSB were purchased from AnaSpec. All solutions were prepared with deionized water (Millipore Milli-Q, 18 MΩ·cm resistivity).

In the present studies we have chosen to work at pH 7.4, where aggregation and fibrillogenesis occur for Aβ12-28-Cys. The estimated isoelectric point of the Aβ12-28-Cys is about pI 7.9.[31] Dissolving the peptide up to millimolar concentrations directly into an ice-cold aqueous solvent at pH 7.4, which is close to the isoelectric point of peptide, gives a sample with reproducible and stable spectral properties. A pH 7.4, phosphate buffer in aqueous solution was prepared with 50 mM Na_2HPO_4, 50 mM KH_2PO_4. 5 mM solution of the redox probe, $[Fe(CN)_6]^{3-/4-}$, was prepared with 1:1 molar ratio of $K_3[Fe(CN)_6]$ and $K_4[Fe(CN)_6]$ in phosphate buffer at pH 7.4. Aβ12-28-Cys peptide stock solution was prepared in 50 mM phosphate buffer solution pH 7.4 and stored at −20 °C, or diluted with buffer at pH 7.4 to prepare solutions of different concentrations, which were stored at 4 °C. The electrodes were protected from water evaporation and kept at 4 °C for 72 h.

2.2. Peptide Immobilization on the Surface. Gold electrodes (99.99% (w/w), polycrystalline) were purchased from CH Instruments Inc. (Austin, TX). Prior to experiments, the gold electrode was immersed for 5 min into a piranha solution (1:3, v/v, 30% H_2O_2, 18 M H_2SO_4). The electrode was then polished with wet 0.05 μm alumina slurry on a flat pad for at least 2 min.

Upon rinsing with Millipore water, the electrodes were then dipped in 0.5 M KOH solution, cycled between −0.1 and −1.5 V (vs Ag/AgCl) at a scan rate of 0.1 V s^{-1}. At the completion of the scan the electrode was once again rinsed with Millipore water. The electrode was cleaned by electrochemical sweeping in 0.5 M H_2SO_4 by cycling at a scan rate of 0.1 V s^{-1} from a potential of −0.1 to +1.6 V (vs Ag/AgCl) until a stable gold oxidation peak at 1.1 V was obtained.

Subsequently, the gold electrode was placed in ethanol for 5 min with ultrasonication and then dried with N_2. The clean gold electrode was incubated with 50 μM Aβ12-28-Cys peptide in phosphate buffer solution (50 mM Na_2HPO_4, 50 mM KH_2PO_4, pH 7.4) for 72 h at 4 °C. Afterward, the electrode was rinsed with phosphate buffer solution and dried with N_2. Subsequently, the peptide-modified electrode was incubated with 5 mM solution of CR and BSB in phosphate buffer solution (50 mM, pH 7.4) at room temperature.

2.3. Electrochemical Instrumentation and Measurements. All electrochemical studies, including cyclic voltammetry (CV), square wave voltammetry (SWV), and electrochemical impedance spectroscopy (EIS), were performed with an electrochemical analyzer (CH Instruments 660B, Austin, TX) connected to a personal computer. All measurements were carried out at room temperature in an enclosed and grounded Faraday cage. A conventional three-electrode system was used, comprising a peptide-modified gold electrode as a working electrode, a platinum wire as a counter electrode, and Ag/AgCl/3 M KCl as a reference electrode. The reference electrode was always isolated from the cell by a miniature salt bridge (agar plus KNO_3) to avoid the leakage of the Cl^- ions from the reference electrode to the measurement system. The open-circuit potential (OCP) of the system was measured prior to all electrochemical experiments to prevent sudden potential related changes in the film. All electrochemical measurements were started from OCP and were carried out in 50 mM phosphate buffer solution pH 7.4 and 5 mM $[Fe(CN)_6]^{3-/4-}$. All CV experiments were performed at a scan rate of 0.1 V s^{-1} in the range from −0.1 to +0.6 V. SWV experiments were carried out in the same

dx.doi.org/10.1021/la300093h | *Langmuir* 2012, 28, 6377−6385

range as CV with a step potential of 5 mV, pulse amplitude of 25 mV, and a frequency of 15 Hz. The EIS measurements were recorded within the frequency range of 0.1 Hz to 100 kHz at the formal potential of the redox couple $[Fe(CN)_6]^{3-/4-}$ (250 mV) with ac amplitude of 10 mV. The experimental EIS data were fitted to an appropriate equivalent circuit using the software ZView 3.2c by Scribner Associates Inc.

2.4. Surface Characterization. Fourier transform reflection absorption infrared spectroscopy (FT-RAIRS) was carried out using a Thermo Nicolet NEXUS 670 FT-IR. A peptide film was prepared by adsorption of the peptide at the cysteine thiol group onto the gold substrate. A 100 nm thick gold substrate prepared by electron-beam deposition with a prior 5 nm thick titanium adhesion layer on a cleaned Si wafer having a 1 μm thick SiO_2 layer.

Prior to incubation of Aβ12-28-Cys peptide on the gold-coated silicon, few drop of piranha solution (H_2SO_4 70%:H_2O_2 30% = 3:1, v/v) was deposited for 2 min on the surface, and then the gold-coated silicon surface was washed and sonicated sequentially in methanol and deionized water for 10 min each. Finally, the electrode was dried with N_2 flow. Aβ12-28-Cys film was prepared by soaking a clean gold substrate for 72 h at the 4 °C temperature in a phosphate-buffered solution (50 mM Na_2HPO_4, 50 mM KH_2PO_4, pH 7.4) of the peptide (0.1 mg/mL). The same molar as peptide were used for 60 min interaction of CR and BSB with peptide film.

2.5. ThT Fluorescence Assay. Solutions of Aβ12-28-Cys (50 μM, dissolved in 50 mM phosphate buffer) were incubated for fibril growth for 4 days. Solutions of CR and BSB were added to the Aβ12-28-Cys fibril sample in 1:1 (CR or BSB: Aβ12-28-Cys) molar ratio. Thioflavin T (ThT) was added to the samples to the final concentration of 50 μM in 96-well plates. The resulting ThT fluorescence of samples was measured at an emission of 485 nm using the excitation wavelength 440 using a Bio-Tek Synergy HT Multimode Microplate Reader.

2.6. Transmission Electron Microscopy. Samples were prepared in 50 mM phosphate buffer solution (50 mM Na_2HPO_4, 50 mM KH_2PO_4, pH 7.4) and then dried onto carbon-coated nickel grids for characterization by transmission electron microscopy (TEM) (JEOL 1200 EX) operated at 80 kV. TEM was used for the characterization of Aβ12-28-Cys peptide solution samples in the course of aggregation.

2.7. Optimization of Experimental Conditions. In order to establish optimal conditions for the peptide film formation, cyclic voltammetry (CV) was carried out for an electroactive species such as $[Fe(CN)_6]^{3-/4-}$ at a film of Aβ12-28-Cys on gold electrodes. The peptide film on the electrode surface is globally uncharged and does not affect the electron transfer from the negatively charged redox ions, such as $[Fe(CN)_6]^{3-/4-}$, to the electrode.

The extent of kinetic hindrance to the electron transfer process increases with the increasing coverage and thickness and the decreasing defect density of the barrier.[32] The influence of incubation time on CV signal was investigated for modified gold electrode with Aβ12-28-Cys in 5 mM $[Fe(CN)_6]^{3-/4-}$ solution. The results show (Figure 1) that the current of the modified electrodes decreased with the increment of incubation time and then leveled off after 60 h (Figue S1), implying that the Aβ12-28-Cys modified electrodes were saturated with Cys-Aβ12-28. Therefore, 72 h was selected as the optimum incubation time.

Figure 2 shows the effect of Aβ12-28-Cys peptide concentration on cyclic voltammogram response after 72 h incubation on gold electrodes. By increasing the concentration of Aβ12-28-Cys peptide from 5 nM to 50 μM, the measured current of gold electrode was decreased corresponding to the concentration of Aβ12-28-Cys peptide. When the concentration of Aβ12-28-Cys peptide is higher than 20 μM, changes in current response become sluggish, which might be attributed to the limitation of active sites for peptide bonding (Figure S2). Thus, Aβ12-28-Cys peptide concentration of 50 μM (103 μg/mL) was chosen in the experiment for film preparation.

3. RESULTS AND DISCUSSION

3.1. Film Characterization. CV and SWV were employed to characterize the film by monitoring the electron transfer process on the Aβ12-28-Cys peptide film on gold electrodes in the presence of $[Fe(CN)_6]^{3-/4-}$ as a redox probe.

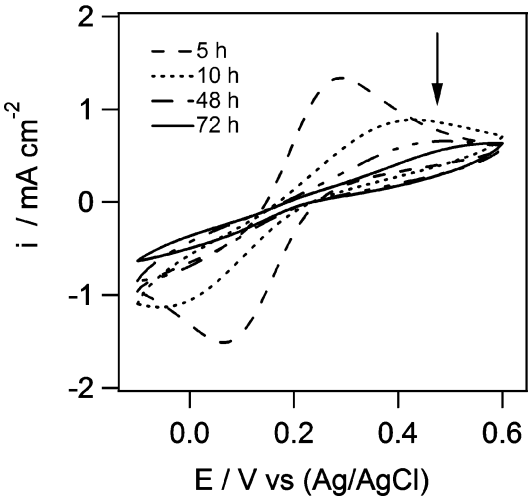

Figure 1. Influence of incubation time on cyclic voltammograms of a gold electrode incubated with 50 μM Aβ12-28-Cys. Cyclic voltammograms were run in a 5 mM $[Fe(CN)_6]^{3-/4-}$ (1:1) solution in phosphate buffer (50 mM Na_2HPO_4, 50 mM KH_2PO_4, pH 7.4) at scan rate of 0.1 V s^{-1}. The voltage range was −0.1 to 0.6 V.

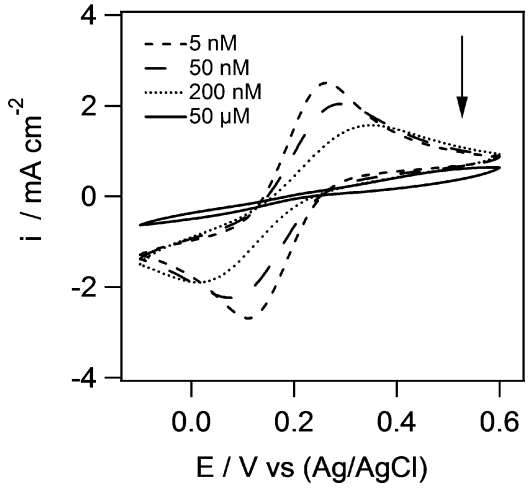

Figure 2. Influence of Aβ12-28-Cys concentration on cyclic voltammogram responses after 72 h incubation. CVs were run in 5 mM $[Fe(CN)_6]^{3-/4-}$ (1:1) solution in phosphate buffer (50 mM Na_2HPO_4, 50 mM KH_2PO_4, pH 7.4) at scan rate of 0.1 V s^{-1}.The voltage range was −0.1 to 0.6 V.

In order to facilitate the Aβ12-28-Cys peptide immobilization on the gold electrode surface, this process was carried out in buffered solution. The isoelectric point (pI) of Aβ12-28 peptide is 7.9,[31] so at pH 7.4 it is globally uncharged by carry 3 positive and 3 negative charges. The CVs obtained for bare and modified gold electrodes are presented in Figure 3. Electrochemical analysis showed that well-packed peptide films were formed by means of assembling cysteine-terminated peptides onto the gold electrode. The voltammograms obtained for the peptide-coated electrode lacked the characteristic redox waves observed in the voltammogram of the stripped gold electrode, suggesting that densely packed peptidic films are formed.

3.2. EIS Analysis. EIS has been exploited in sensor applications, biological cell analysis, and clinical analysis.[33] However, it has been rarely applied to the investigation of the

dx.doi.org/10.1021/la300093h | Langmuir 2012, 28, 6377−6385

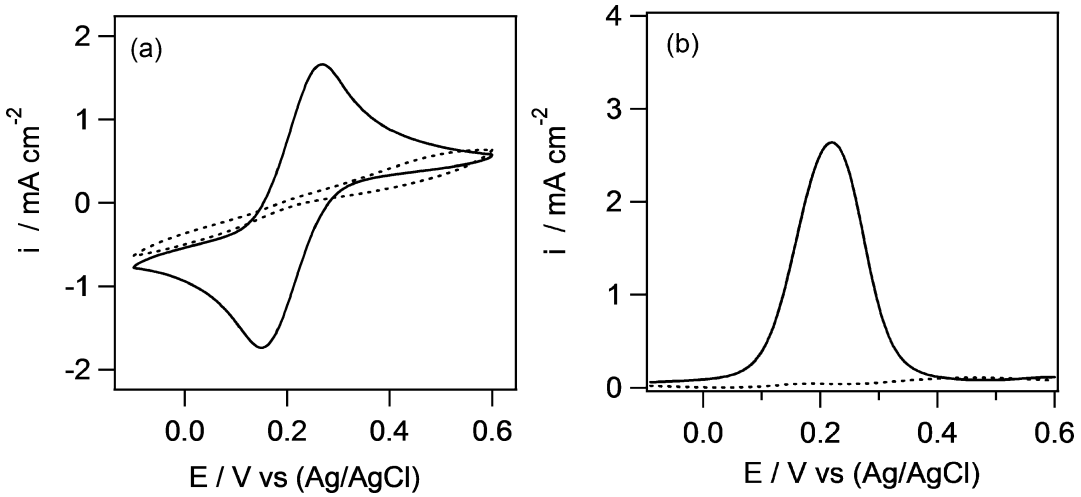

Figure 3. (a) Cyclic voltammograms and (b) square-wave voltammograms of bare gold (solid line) and gold modified with Aβ12-28-Cys (dotted line) after 72 h incubation of bare gold in 50 μM Aβ12-28-Cys. The solution composition was 5 mM $[Fe(CN)_6]^{3-/4-}$ (1:1) in phosphate buffer (50 mM Na_2HPO_4, 50 mM KH_2PO_4, pH 7.4) at scan rate of 0.1 V s^{-1}. The voltage range was −0.1 to 0.6 V.

interaction of molecules with Aβ peptide. In EIS, a small sinusoidal voltage is applied, and the respondent current is collected within a frequency range, allowing the evaluation of the impedance, Z, which may give the information on the under laying system.[34]

Figure 4 shows the typical Nyquist plot of a bare and peptide modified gold electrode in phosphate buffer (50 mM Na_2HPO_4, 50 mM KH_2PO_4, pH 7.4), containing 5 mM $[Fe(CN)_6]^{3-/4-}$ as a redox probe at an applied potential of 250 mV vs Ag/AgCl in a frequency range of from 0.1 Hz to 100 kHz. In the figure, the highest and lowest frequencies are measured and the characteristic frequency (the frequency at which the imaginary component of the impedance has a maximum) has been labeled, since the frequency dependence is obscured in a Nyquist plot.[34]

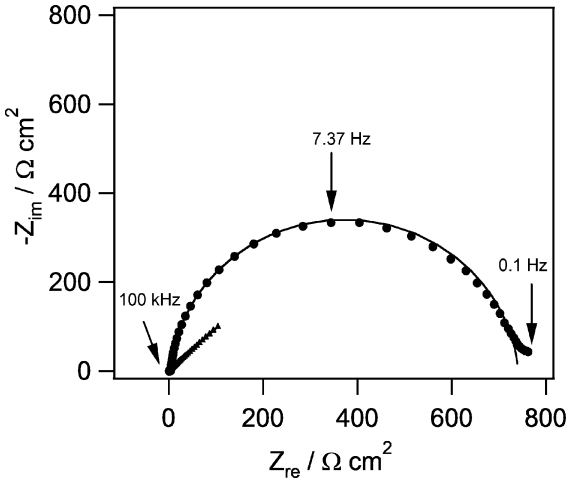

Figure 4. Representative Nyquist plots ($-Z_{im}$ vs Z_{re}) for (▲) bare gold electrode (●) after 72 h incubation of bare gold electrode in 50 μM Aβ12-28-Cys peptide in phosphate buffer (50 mM Na_2HPO_4, 50 mM KH_2PO_4, pH 7.4). Measured data are shown as symbols with calculated fit to the equivalent circuit (Figure 5b) as solid lines. Impedance spectra obtained in phosphate buffer (50 mM Na_2HPO_4, 50 mM KH_2PO_4, pH 7.4), containing 5 mM $[Fe(CN)_6]^{3-/4-}$ (1:1) as a redox probe, at a formal potential of 250 mV vs Ag/AgCl, frequency range from 100 kHz to 0.1 Hz, and ac amplitude of 10 mV.

As shown in Figure 4, the bare gold electrode exhibits impedance behavior that is characteristic of a mass diffusion controlled electron transfer process.[35] We will focus on the impedance behavior of Aβ12-28-Cys peptide-modified gold electrode. The semicircle at higher frequencies, corresponding to limited electron-transfer process of $[Fe(CN)_6]^{3-/4-}$, occurred after the incubation of gold electrode in Aβ12-28-Cys peptide. This insulating layer on the electrode introduces a barrier to interfacial electron transfer.[36,37] The Aβ12-28-Cys peptide covers the gold surface, effectively blocking the Faradaic current of the redox process of $[Fe(CN)_6]^{3-/4-}$. The EIS data were consistent with the results obtained from CV and SWV experiments (Figure 3) and provide further evidence of peptide film formation on the gold surface and show increases the resistance to charge transfer due to a densely packed film. In Figure 5a, the charge transfer resistance, R_{ct}, and the double layer capacitance, C_{dl}, are associated with the reduction of $[Fe(CN)_6]^{3-/4-}$ on the active surface, while $R_{A\beta}$ and $C_{A\beta}$ are the charge transfer resistance for electron transfer through the film and capacitance of the peptide film, and R_s is the uncompensated resistance of solution. When the film is blocking such that all electron transfer reactions must occur through the film, $R_{A\beta} \gg R_{ct}$, the model of Figure 5a can reduce to Figure 5b where the total resistance, R_t and total capacitance, C_t are given by the equations

$$R_t = \frac{R_{ct}}{\theta} \quad (1)$$

$$C_t = (1 - \theta)C_{A\beta} + \theta C_{dl} \quad (2)$$

where θ is the fraction of the active sites of the surface, which simply relates to the fraction of the peptide coverage by $(1 - \theta)$.

In fitting the EIS data by the equivalent circuit Figure 5b, the total capacitance (C_t) was replaced by a constant phase element (CPE) to account for time constant dispersion as a result of surface inhomogeneity. The CPE is a phenomenological term defined as

$$CPE = [Y_0(j\omega)^{\alpha}]^{-1} \quad (3)$$

dx.doi.org/10.1021/la300093h | Langmuir 2012, 28, 6377−6385

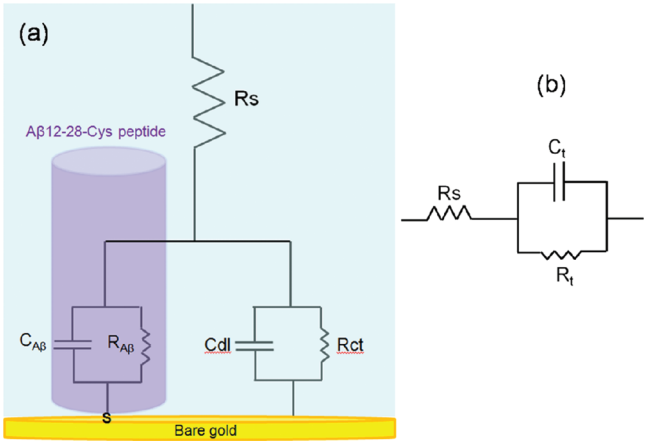

Figure 5. (a) Model representing a partial coverage by a peptide film, and Faradaic process occurring on the active area that is not blocked by the film, and (b) the reduced equivalent circuit used to fit the EIS data. The equivalent electric circuit diagram of the electrochemical interface. R_s: solution resistance; R_{ct}: charge transfer resistance; C_{dl}: double-layer capacitance; $R_{A\beta}$: resistance of the peptide film; $C_{A\beta}$: capacitance of the peptide film; R_t: total resistance; C_t: total capacitance.

where the parameters Y_0 and α are independent of frequency ω and $j^2 = -1$. When $\alpha = 1$, the CPE is identical to a capacitor and $Y_0 = C$. When α is close to unity, the CPE may be converted to capacitance by the equation derived by Brug[38]

$$C_t = \left[Y_0 \left(\frac{1}{R_s} + \frac{1}{R_t} \right)^{\alpha - 1} \right]^{1/\alpha} \quad (4)$$

3.3. Interaction of CR and BSB with Aβ12-28-Cys Peptide Film. The principal components of amyloid plaques are the fibrillar aggregates of β-amyloid (Aβ) peptides (39−43 amino acids), which is one of the main constituents of amyloid plaques in the brains of people suffering from neurodegenerative disease. Aβ readily aggregates into fibrils and plaques.[39,40] Earlier reports indicate that the Aβ12-28 fragment forms fibril aggregates that are toxic.[41]

EIS allows us to monitor the changes occurring at the peptide interface, presumably due to molecular interactions with CR and BSB.[37,42] One has to bare in mind that EIS measurements have to be used in conjunction with other physical measurements described below. The impedance spectra of Aβ12-28-Cys peptide-modified gold electrodes after interaction with 5 mM of CR and BSB are shown in Figures 6a and 6b, respectively. The electrodes were incubated with the compounds studied at different interaction time: 30, 60, 90, and 120 min. The measurements were carried out in electrolyte solution containing 50 mM Na_2HPO_4, 50 mM KH_2PO_4, pH 7.4, and 5 mM $[Fe(CN)_6]^{3-/4-}$. It is important to point out that the impedance behavior of the peptide film after incubation with CR and BSB is significantly different. In the case of CR the impedance decreased with the interaction time, while it increased upon incubation with the BSB peptide.

The equivalent circuit (Figure 5b) was used to fit the experimental data and the results were shown in Figures 6a and 6b as

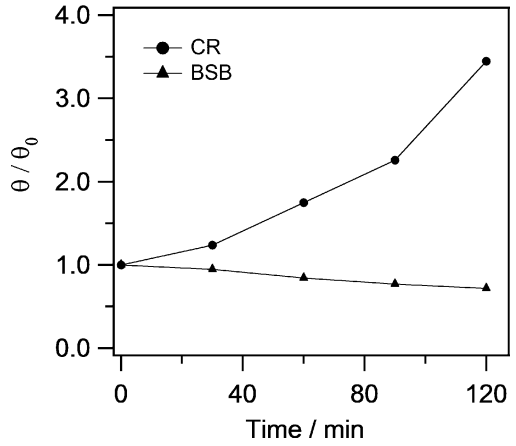

Figure 7. Variation of changes in active sites as a function of reaction time when of Aβ12-28-Cys peptide film interacted with (●) CR and (▲) BSB.

solid lines. It is obvious that the circuit fit the data quite well up to a frequency limit after which mass transport or other processes dominate. The results were summarized in Table 1 for the

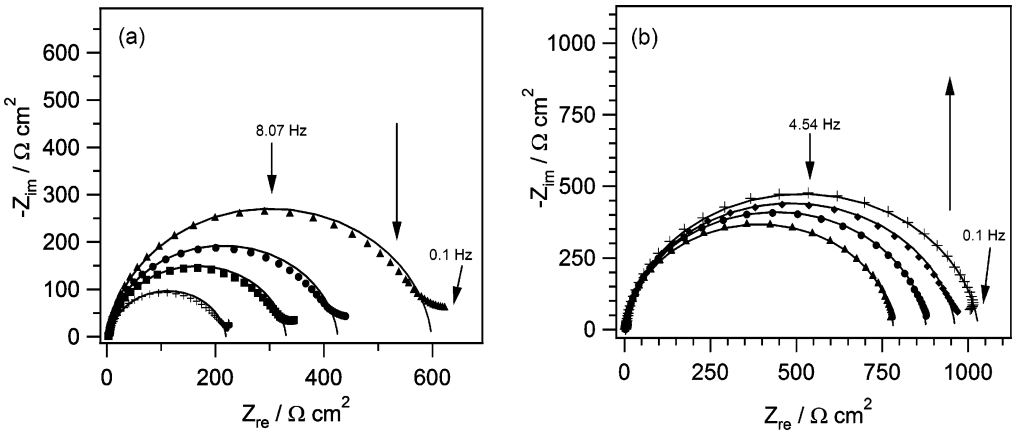

Figure 6. Faradic impedance spectra of for Aβ12-28-Cys peptide film after (▲) 30 min, (●) 60 min, (■) 90 min, and (+) 120 min interaction with 5 mM of (a) Congo red (CR) and (b) β-sheet breaker (BSB) peptide in 50 mM phosphate buffer (pH 7.4). The impedance spectra were recorded from 100 kHz to 0.1 Hz. Measured data are shown as symbols with calculated fit to the equivalent circuit (Figure 5b) as solid lines. Impedance spectra obtained in phosphate buffer (50 mM Na_2HPO_4, 50 mM KH_2PO_4, pH 7.4), containing 5 mM $[Fe(CN)_6]^{3-/4-}$ (1:1) as a redox probe, at a formal potential of 250 mV vs Ag/AgCl, frequency range from 100 kHz to 0.1 Hz, and ac amplitude of 10 mV.

dx.doi.org/10.1021/la300093h | Langmuir 2012, 28, 6377−6385

fittings of Figures 6a and 6b. In both cases, C_t appears not change significantly with interaction time. As illustrated in eq 2, the total capacitance (C_t) is composed of two components: the capacitance of the peptide film ($C_{A\beta}$) and the double-layer capacitance (C_{dl}). When the ratio of the active sites θ changes during the interaction, the first and second term of in eq 2 change in the opposite direction leaving the total capacitance virtually unchanged.

However, the total resistance R_t changed during the interaction, but differently in the case of CR or BSB. Since the rate of $[Fe(CN)_6]^{3-/4-}$ reduction on gold would not be expected to be influenced by CR/BSB interaction, these changes would basically reflect the change in the fraction of active sites during the interaction. The fractional active sites of surface will change as the consequence of reactions of CR or BSB with peptide. Though the EIS cannot provide the absolute values of the fraction of the active sites, the ratio of θ/θ_0 will represent the change in peptide packing with interaction time, which can be obtained via eq 5.

$$\frac{\theta(t)}{\theta_0} = \frac{R(0)}{R(t)} \tag{5}$$

where θ_0 is the fraction of the active area prior to reaction. When $\theta/\theta_0 > 1$, the reaction increases the active area; on the other hand, the active area decreases when $\theta/\theta_0 < 1$.

Figure 7 shows θ/θ_0 as a function of the interaction time of the peptide film with CR and BSB. A significant increase is observed for CR as the interaction time is increased. This indicates that the electron transfer ability of redox probe $[Fe(CN)_6]^{3-/4-}$ was largely improved by the insertion of CR to the peptide film since the θ/θ_0 ratio as a function of time is attributed to the electrostatic repulsion between the solution-based redox probe and the electrode surface. However, the behavior in the presence of BSB is rather different. The ratio of θ/θ_0 decreases with reaction time. This is an indication of a diminished electron transfer from the solution to the electrode surface; therefore, it is difficult for the redox probe $[Fe(CN)_6]^{3-/4-}$ to approach the electrode as compared with the absence of BSB interaction. A decrease in the θ/θ_0 ratio over time is presumably caused by a tighter aggregation caused by the interaction with the BSB peptide. Upon longer BSB interactions, the Aβ12-28-Cys peptide film becomes more dense and crowded. The difference in the electrochemical behavior of the interaction of CR and BSB with Aβ film on the surface might be related to the difference in the mechanism of their interaction with Aβ. According to the literature, two different binding sites (the possible sites on Aβ peptide for CR interaction) have been suggested for CR. In the site with higher affinity, CR orients itself in an antiparallel fashion with respect to the β-sheets and the sulfonate residues of CR align with the N-terminus of peptides to provide ionic interactions between negatively charged sulfonate acid groups of CR and positively charged N-terminus of peptide strands. The second binding site with lower affinity is at the end of fibrils or oligomers and CR orients itself parallel to the β-sheets. Earlier molecular dynamic simulations demonstrated that CR prefers binding antiparallel to the β-sheets which shows that ionic interaction plays an important role in the interaction of CR with amyloid aggregation.[43] Thus, when CR is inserted into the antiparallel β-sheets, it presumably enlarges the distance between the carbonyl oxygen and the amide nitrogen and disrupts the hydrogen bonding between β-sheets. Unlike CR, peptides derived from hydrophobic core of Aβ (Lys-Leu-Val-Phe-Phe) favor binding parallel to the β-sheets at the end of fibrils or oligomers. The interaction of Lys-Leu-Val-Phe-Phe derivatives is presumably through hydrophobic interaction, hydrogen binding, and $\pi-\pi$ stacking with their corresponding residues in the amyloid fibrils or oligomers.[44,45] Hence, it is reasonable to believe that after a long time BSB will accumulate more and bond on the peptide film.

A schematic view of the interactions of Aβ12-28-Cys peptide film on gold with CR and BSB is presented in Scheme 2b,c. Qualitatively, it can be concluded that CR breaks the film as shown by the decrease of the film resistance likely by increasing

Table 1. Values of the Equivalent Circuit Elements Shown in Figure 5b for Aβ12-28-Cys Peptide Film after Different Interaction Time with 5 mM CR and BSB[a]

	R_s/Ω cm^2		C_t/μFcm^{-2}		R_t/Ω cm^2	
time/min	CR	BSB	CR	BSB	CR	BSB
0	3.6 ± 0.06	3.8 ± 0.11	19.6 ± 2.60	19.6 ± 2.80	738 ± 11	738 ± 13
30	3.2 ± 0.08	3.6 ± 0.28	24.2 ± 3.91	22.4 ± 2.82	595 ± 15	780 ± 17
60	3.5 ± 0.11	3.0 ± 0.10	25.7 ± 4.31	22.0 ± 7.50	422 ± 43	875 ± 5
90	3.5 ± 0.22	3.2 ± 0.47	25.9 ± 2.00	19.5 ± 2.00	327 ± 15	959 ± 14
120	5.5 ± 0.25	4.1 ± 0.89	19.2 ± 0.64	24.2 ± 0.85	214 ± 12	1026 ± 20

[a]The solution composition was 5 mM $[Fe(CN)_6]^{3-/4-}$ (1:1) in phosphate buffer (50 mM Na_2HPO_4, 50 mM KH_2PO_4, pH 7.4) at 250 mV (vs Ag/AgCl). Errors given are standard deviations for three different day measurements and fitting error was less than 5%.

Scheme 2. (a) Schematic View Showing the Aβ12-28-Cys Peptide Adsorption onto Gold Surfaces Followed by the Interactions with (b) Congo Red (CR) and (c) β-Sheet Breaker Peptide (BSB)

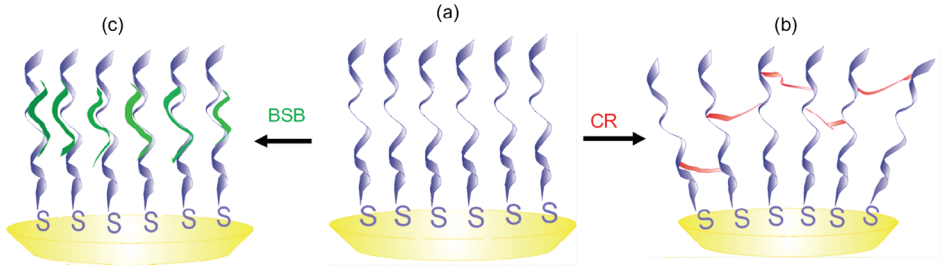

dx.doi.org/10.1021/la300093h | Langmuir 2012, 28, 6377−6385

its porosity, whereas BSB makes the film more compact and thicker increasing the resistance

The EIS results are in agreement with the CV observations, which showed that the current decreases/increase with interaction of BSB and CR, corresponding to the observed increase/decrease in ability of redox probe $[Fe(CN)_6]^{3-/4-}$ (Figure S3). The response of Aβ12-28-Cys peptide film for different concentrations of CR and BSB was also investigated (Figure S4). The EIS results showed that at lower concentration of BSB a smaller diameter of the semicircle was observed, and as the concentration was increased, the resulting diameter of the semicircle was increased. The opposite is observed in the case of the interaction of CR with the peptide film.

Fourier transform reflection absorption infrared spectroscopy (FT-RAIRS) provides structural information and provides a spectroscopic signature for β-sheet structures. Infrared spectra of the solid states of Aβ12-28-Cys, BSB, and CR are shown in Figure S5. Our Aβ12-28-Cys peptide modified gold substrates showed the presence of an intense band at 1624 cm^{-1} and a weak band at 1692 cm^{-1} in the amide I region (Figure 8a),

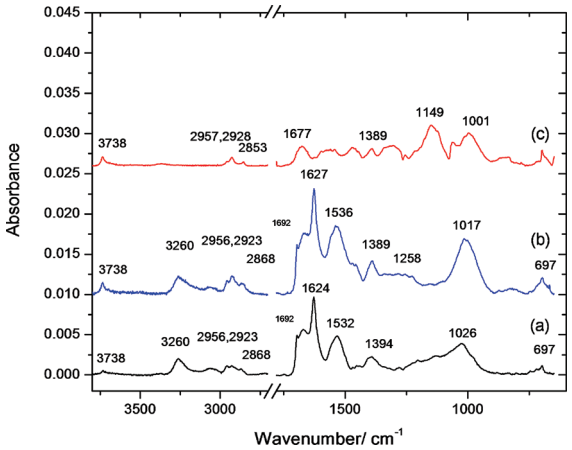

Figure 8. FT-RAIRS of Aβ12-28-Cys modified gold substrates before (a) and after interacting with 50 μM BSB peptide (b) and CR (c), separately for 120 min in phosphate buffer (50 mM Na_2HPO_4, 50 mM KH_2PO_4, pH 7.4).

indicating that the peptides are arranged predominantly as an antiparallel β-sheet. Antiparallel β-sheets are commonly characterized by a pair of amide I bands at 1615−1620 and 1680−1690 cm^{-1}.[46] An additional band at 3260 cm^{-1} is for NH groups involved in β-sheet-like H-bonds.[47] Figure 8b also shows that there are differences between the spectra of BSB treated Aβ12-28-Cys modified gold substrate and Aβ12-28-Cys modified gold substrate. The bands at 1624 and 1692 cm^{-1} showed little change in positions, rather a slightly enhanced absorbance for BSB treated Aβ12-28-Cys modified gold substrate, indicating the presence of β-sheet conformation. These bands were completely absent for CR treated Aβ12-28-Cys modified gold substrate (Figure 8c). Instead, the appearance of the new band at 1677 cm^{-1} and absence of H-bonded NH groups clearly demonstrated a conformational change to the random coil state. Frequencies above 1660 cm^{-1} have been assigned to random coil structures of peptide and proteins.[48,49]

The amyloidogenic properties of Aβ12-28-Cys and its interaction with CR and BSB were also confirmed in solution by transmission electron microscopy (TEM) and thioflavin T (ThT) fluorescence. TEM of aggregated/precipitated peptide samples obtained from aqueous solutions showed the typical fibrillar structure of β-amyloid peptides (Figure 9a).

Equimolar amounts of the BSB peptide and CR were added separately to solutions of preformed fibrils of Aβ12-28-Cys, incubated for 4 days, and imaged by TEM. Our results show that preformed fibrils maintain their integrity with the BSB peptide (Figure 9c), but addition of CR causes a complete dissolution (Figure 9b). These observations are consistent with previous studies.[13,16] BSBs prevent the fibril formation in a freshly prepared solution of amyloid peptides when used in equimolar quantities.[16] But the dissolution of a significant fraction of preformed fibrils occurs in the presence of a high excess (up to 20 times) of BSBs,[10] possibly because of the stabilization of the monomeric species and shift of the dynamic equilibrium that exists between the fibrils and different active species.[9]

Thioflavin T (ThT) fluorescence has been widely used for probing Aβ aggregation and inhibition.[50,51] Monitoring the ThT fluorescence at 485 nm which occurs after its binding to amyloid fibril is an effective method to probe Aβ fibril formation. Solutions of CR and BSB were added to the preformed Aβ12-28-Cys fibrils in a 1:1 (CR or BSB:Aβ12-28-Cys) molar ratio. Upon addition of CR to Aβ12-28-Cys, the ThT fluorescence of Aβ12-28-Cys samples decreased immediately. This dramatic decrease might not directly be explained as the reduction of Aβ fibrils due to the competition of CR and ThT to bind to the same binding sites at Aβ12-28-Cys. Therefore, we assumed that ThT fluorescence reading in the presence of CR might be bias. Similar behavior was previously reported for ThT flouresence of Aβ samples in the presence of other dyes such as resveratrol.[52] In contrast to CR, the ThT fluorescence of Aβ solutions slightly increased following the addition of BSB to amyloid fibrils (BSB:Aβ 1:1, see Supporting Information). This increase is in good agreement with our electrochemical and TEM results.

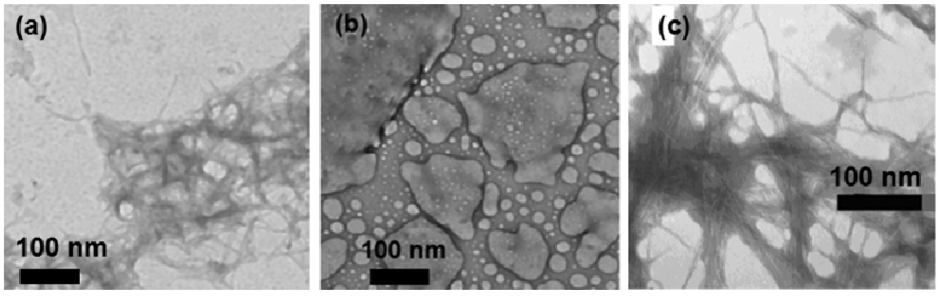

Figure 9. (a) Transmission electron microscopy (TEM) image observation of Aβ12-28-Cys peptides in the absence of CR and BSB, (b) after addition of CR and (c) after addition of BSB incubated for 4 days in phosphate buffer (50 mM Na_2HPO_4, 50 mM KH_2PO_4, pH 7.4).

dx.doi.org/10.1021/la300093h | *Langmuir* 2012, 28, 6377−6385

In conclusion, our studies provide information about translocation or blockade events of Aβ12-28-Cys peptide film in the presence of CR or BSB and interpret deference in these changes by different techniques.

4. CONCLUSIONS

In this work, we demonstrated that, in addition to more classical spectroscopic techniques, electrochemical methods including electrochemical impedance spectroscopy provide some useful information about differences in the interactions of CR and BSB with Aβ12-28-Cys peptide immobilized on gold surfaces and in fact can be used to monitor this interaction. However, the net result of the interaction is fundamentally different indicating differences in the interaction and in film structure upon exposure. CR appears to cause loss of film integrity, making the film more permeable to solution based redox probes. In contrast, BSB appears to integrate into the film and cause an increase in the resistance to charge transfer. We interpret these differences in terms of structural differences in the film structure. CR appears to lead to porous peptide films, whereas the opposite is the case for BSB. FT-RAIRS studies further support the interaction of peptide films with CR or BSB. Clearly our studies indicate the value of EIS measurements for monitoring interactions of Aβ disrupting molecules with peptide films. Nonelectrochemical techniques such as TEM and ThT fluorescence measurements provide complementary information that support our chemical understanding gained from our electrochemical investigations. Additional studies are ongoing screening larger peptide libraries and their abilities to interact with peptide films.

■ ASSOCIATED CONTENT

Ⓢ Supporting Information

Influence of the incubation time and concentration on cyclic voltammograms of Aβ12-28-Cys, electrochemical impedance spectra of Aβ12-28-Cys in the presence of different concentrations of CR and BSB, ellipsometry measurement, X-ray photoelectron spectroscopy analyses, and ThT fluorescence results. This material is available free of charge via the Internet at http://pubs.acs.org.

■ AUTHOR INFORMATION

Notes

The authors declare no competing financial interest.

■ ACKNOWLEDGMENTS

We thank the Natural Science and Engineering Research Council of Canada for financial support. In addition, we thank Dr. Mark Biesinger at Surface Science Western at the University of Western Ontario for XPS measurements.

■ REFERENCES

(1) Hardy, J.; Selkoe, D. J. The Amyloid Hypothesis of Alzheimer's Disease: Progress and Problems on the Road to Therapeutics. *Science* **2002**, *297*, 353−356.

(2) Selkoe, D. J. Alzheimer's Disease Is a Synaptic Failure. *Science* **2002**, *298*, 789−791.

(3) Brambilla, D.; Le Droumaguet, B.; Nicolas, J.; Hashemi, S. H.; Wu, L.-P.; Moghimi, S. M.; Couvreur, P.; Andrieux, K. Nanotechnologies for Alzheimer's Disease: Diagnosis, Therapy, and Safety Issues. *Nanomedicine* **2011**, *7*, 521−540.

(4) Necula, M.; Kayed, R.; Milton, S.; Glabe, C. G. Small Molecule Inhibitors of Aggregation Indicate That Amyloid β Oligomerization and Fibrillization Pathways Are Independent and Distinct. *J. Biol. Chem.* **2007**, *282*, 10311−10324.

(5) Merlini, G.; Ascari, E.; Amboldi, N.; Bellotti, V.; Arbustini, E.; Perfetti, V.; Ferrari, M.; Zorzoli, I.; Marinone, M.; Garini, P. Interaction of the Anthracycline 4′-iodo-4′-deoxydoxorubicin with Amyloid Fibrils: Inhibition of Amyloidogenesis. *Proc. Natl. Acad. Sci. U. S. A.* **1995**, *92*, 2959−2963.

(6) Tomiyama, T.; Shoji, A.; Kataoka, K.; Suwa, Y.; Asano, S.; Kaneko, H.; Endo, N. Inhibition of Amyloid β Protein Aggregation and Neurotoxicity by Rifampicin: Its Possible Function As a Hydroxyl Radical Scavenger. *J. Biol. Chem.* **1996**, *271*, 6839−6844.

(7) Pappolla, M.; Bozner, P.; Soto, C.; Shao, H.; Robakis, N. K.; Zagorski, M.; Frangione, B.; Ghiso, J. Inhibition of Alzheimer β-Fibrillogenesis by Melatonin. *J. Biol. Chem.* **1998**, *273*, 7185−7188.

(8) Hilbich, C.; Kisters-Woike, B.; Reed, J.; Masters, C. L.; Beyreuther, K. Substitutions of Hydrophobic Amino acids Reduce the Amyloidogenicity of Alzheimer's Disease βA4 Peptides. *J. Mol. Biol.* **1992**, *228*, 460−473.

(9) Soto, C.; Kindy, M.; Baumann, M.; Frangione, B. Inhibition of Alzheimer's Amyloidosis by Peptides That Prevent β-Sheet Conformation. *Biochem. Biophys. Res. Commun.* **1996**, *226*, 672−680.

(10) Soto, C.; Sigurdsson, E. M.; Morelli, L.; Kumar, A.; Castano, E. M.; Frangione, B. β-sheet Breaker Peptides Inhibit Fibrillogenesis in a Rat Brain Model of Amyloidosis: Implications for Alzheimer's therapy. *Nat. Med.* **1998**, *4*, 822−826.

(11) Masuda, M.; Suzuki, N.; Taniguchi, S.; Oikawa, T.; Nonaka, T.; Iwatsubo, T.; Hisanaga, S.; Goedert, M. Small Molecule Inhibitors of α-synuclein Filament Assembly. *Biochemistry* **2006**, *45*, 6085−6094.

(12) Taniguchi, S.; Suzuki, N.; Masami Masuda, M.; Hisanaga, S. I.; Iwatsubo, T.; Goedert, M.; Hasegawa, M. Inhibition of Heparin-induced Tau Filament Formation by Phenothiazines, Polyphenols, and Porphyrins. *J. Biol. Chem.* **2005**, *280*, 7614−7623.

(13) Frid, P.; Anisimov, S. V.; Popovic, N. Congo red and Protein Aggregation in Neurodegenerative Diseases. *Brain Res. Rev.* **2007**, *53*, 135−160.

(14) Carter, D. B.; Chou, K. C. A Model for Structure-Dependent Binding of Congo Red to Alzheimer β-Amyloid Fibrils. *Neurobiol. Aging* **1998**, *19*, 37−40.

(15) Permanne, B.; Adessi, C.; Fraga, S.; Frossard, M. J.; Saborio, G. P.; Soto, C. Are Beta-sheet Breaker Peptides Dissolving the Therapeutic Problem of Alzheimer's Disease? *J. Neural Transm., Suppl.* **2002**, *62*, 293−301.

(16) Tjernberg, L. O.; Naslund, J.; Lindqvist, F.; Johansson, J.; Karlstrom, A. R.; Thyberg, J.; Terenius, L. Arrest of β-Amyloid Fibril Formation by a Pentapeptide Ligand. *J. Biol. Chem.* **1996**, *271*, 8545−8548.

(17) Soto, C.; Castano, E. M.; Frangione, B.; Inestrosa, N. C. The α-Helical to β-Strand Transition in the Amino-terminal Fragment of the Amyloid β-Peptide Modulates Amyloid Formation. *J. Biol. Chem.* **1995**, *270*, 3063−3067.

(18) Wood, S. J.; Wetzel, R.; Martin, J. D.; Hurle, M. R. Prolines and Amyloidogenicity in Fragments of the Alzheimers Peptide Beta/A4. *Biochemistry* **1995**, *34*, 724−730.

(19) Gordon, D. J.; Tappe, R.; Meredith, S. C. Design and Characterization of a Membrane Permeable *N*-methyl Amino Acid-containing Peptide that Inhibits Aβ1−40 Fibrillogenesis. *J. Pept. Res.* **2002**, *60*, 37−55.

(20) Rabanal, F.; Tusell, J. M.; Sastre, L.; Quintero, M. R.; Cruz, M.; Grillo, D. Structural, Kinetic and Cytotoxicity Aspects of 12-28 β-amyloid Protein Fragment: A Reappraisal. *J. Pept. Sci.* **2002**, *8*, 578−588.

(21) Jarvet, J.; Damberg, P.; Bodell, K.; Erikson, L. E. G.; Graslund, A. Reversible Random Coil to β-Sheet Transition and the Early Stage of Aggregation of the Aβ(12-28) Fragment from the Alzheimer Peptide. *J. Am. Chem. Soc.* **2000**, *122*, 4261−4268.

(22) Gabrielli, C. *Use and Application of Electrochemical Impedance Techniques*; Solartron Analytica: Farnborough, UK, 1990.

(23) Katz, E.; Willner, I. Probing Biomolecular Interactions at Conductive and Semiconductive Surfaces by Impedance Spectroscopy:

Routes to Impedimetric Immunosensors, DNA-Sensors, and Enzyme Biosensors. *Electroanalysis* **2003**, *15*, 913−947.
(24) Baba, A.; Park, M. K.; Advincula, R. C.; Knoll, W. Simultaneous Surface Plasmon Optical and Electrochemical Investigation of Layer-by-Layer Self-Assembled Conducting Ultrathin Polymer Films. *Langmuir* **2002**, *18*, 4648−4652.
(25) Schlereth, D. D. Characterization of Protein Monolayers by Surface Plasmon Resonance Combined with Cyclic Voltammetry 'In Situ'. *J. Electroanal. Chem.* **1999**, *464*, 198−207.
(26) McMasters, M. J.; Hammer, R. P.; McCarley, R. L. Surface-Induced Aggregation of Beta Amyloid Peptide by ω-Substituted Alkanethiol Monolayers Supported on Gold. *Langmuir* **2005**, *21*, 4464−4470.
(27) Kowalewski, T.; Holtzman, M. D. In Situ Atomic Force Microscopy Study of Alzheimer's Beta-amyloid Peptide on Different Substrates: New Insights into Mechanism of Beta-sheet Formation. *Proc. Natl. Acad. Sci. U. S. A.* **1999**, *96*, 3688−3693.
(28) Flätgen, G.; Krischer, K.; Pettinger, B.; Doblhofer, K.; Junkes, H.; Ertl, G. Two-Dimensional Imaging of Potential Waves in Electrochemical Systems by Surface Plasmon Microscopy. *Science* **1995**, *296*, 668−671.
(29) Boussaad, S.; Pean, J.; Tao, N. High-Resolution Multi-wavelength Surface Plasmon Resonance Spectroscopy for Probing Conformational and Electronic Changes in Redox Proteins. *Anal. Chem.* **2000**, *72*, 222−226.
(30) Cui, X.; Jiang, D.; Diao, P.; Li, J.; Tong, R.; Wang, X. Assessing the Apparent Effective Thickness of Alkanethiol Self-assembled Monolayers in Different Concentrations of $Fe(CN)_6^{3-}/Fe(CN)_6^{4-}$ by Ac Impedance Spectroscopy. *J. Electroanal. Chem.* **1999**, *470*, 9−13.
(31) Yokoyama, K.; Welchons, D. R. The Conjugation of Amyloid Beta Protein on the Gold Colloidal Nanoparticles Surfaces. *Nanotechnology* **2007**, *18*, No.105101
(32) Bard, A. J.; Faulkner, L. R. *Electrochemical Methods; Fundamentals and Applications*; Wiley: New York, 2001.
(33) Grieshaber, D.; MacKenzie, R.; Vörös, J.; Reimhult, E. Electrochemical Biosensors-Sensor Principles and Architectures. *Sensors* **2008**, *8*, 1400−1458.
(34) Gileadi, E. *Electrode Kinetics for Chemists, Chemical Engineers and Material Scientists*; VCH: New York, 1993.
(35) Liu, S.; Liu, J.; Han, X.; Cui, Y.; Wang, W. Electrochemical synthesis of gold nanostructure modified electrode and its development in electrochemical DNA biosensor. *Biosens. Bioelectron.* **2010**, *25*, 1640−1645.
(36) Campuzano, S.; Pedrero, M.; Montemayor, C.; Fatás, E.; Pingarrón, J. M. Characterization of Alkanethiol-self-assembled Monolayers-modified Gold Electrodes by Electrochemical Impedance Spectroscopy. *J. Electroanal. Chem.* **2006**, *586*, 112−121.
(37) Wang, L.; Wang, E. Direct Electron Transfer between Cytochrome c and a Gold Nanoparticles Modified Electrode. *Electrochem. Commun.* **2004**, *6*, 49−54.
(38) Brug, G. J.; Van den Eeden, A. L. G.; Sluyters-Rehbach, M.; Sluyters, J. H. The Analysis of Electrode Impedances Complicated by the Presence of a Constant Phase Element. *J. Electroanal. Chem. Interfacial Electrochem.* **1984**, *176*, 275−295.
(39) Haass, C.; Schlossmacher, M. G.; Hung, A. Y.; Vigo-Pelfrey, C.; Mellon, A.; Ostaszewski, B. L.; Lieberburg, I.; Koo, E. H.; Schenk, D.; Teplow, D. B. Amyloid β-peptide is Produced by Cultured Cells During Normal Metabolism. *Nature* **1992**, *359*, 322−325.
(40) Shoji, M.; Golde, T. E.; Ghiso, J.; Cheung, T. T.; Estus, S.; Shaffer, L. M.; Cai, X. D.; McKay, D. M.; Tintner, R. Production of the Alzheimer Amyloid β Protein by Normal Proteolytic Processing. *Science* **1992**, *258*, 126−129.
(41) Fraser, P. E.; Levesque, L.; McLachlan, D. R. Alzheimer Aβ amyloid Forms an Inhibitory Neuronal Substrate. *J. Neurochem.* **1994**, *62*, 1227−1230.
(42) Long, Y.; Nie, L.; Chen, J.; Yao, S. Piezoelectric Quartz Crystal Impedance and Electrochemical Impedance Study of HSA−diazepam Interaction by Nanogold-structured Sensor. *J. Colloid Interface Sci.* **2003**, *263*, 106−112.
(43) Wu, C.; Wang, Z.; Lei, H.; Zhang, W.; Duan, Y. Dual Binding Modes of Congo Red to Amyloid ProtofibrilSurface Observed in Molecular Dynamics Simulation. *J. Am. Chem. Soc.* **2007**, *129*, 1225−1232.
(44) Ma, B.; Nussinov, R. Stabilities and Conformations of Alzheimer's β-amyloid Peptide Oligomers (Aβ_{16-22}, Aβ_{16-35}, and Aβ_{10-35}): Sequence Effects. *Proc. Natl. Acad. Sci. U. S. A.* **2002**, *99*, 14126−14131.
(45) Luhrs, T.; Ritter, C.; Adrian, M.; Riek-Loher, D.; Bohrmann, B.; Dobeli, H.; Schubert, D.; Riek, R. 3D Structure of Alzheimer's Amyloid-β(1−42) Fibrils. *Proc. Natl. Acad. Sci. U. S. A.* **2005**, *102*, 17342−17347.
(46) Krimm, S.; Bandekar, J. Vibrational Spectroscopy and Conformation of Peptides, Polypeptides, and Proteins. *Adv. Protein Chem.* **1986**, *38*, 181−364.
(47) Mandal, H. S.; Kraatz, H.-B. Effect of the surface curvature on the secondary structure of peptides adsorbed on nanoparticles. *J. Am. Chem. Soc.* **2007**, *129*, 6356−6357.
(48) Dyer, R. B.; Gai, F.; Woodruff, W. H.; Gilmanshin, R.; Callender, R. H. Infrared Studies of Fast Events in Protein Folding. *Acc. Chem. Res.* **1998**, *31*, 709−716.
(49) Gilmanshin, R.; Williams, S.; Callender, R. H.; Woodruff, W. H.; Dyer, R. B. Fast Events in Protein Folding: Relaxation Dynamics and Structure of the I Form of Apomyoglobin. *Biochemistry* **1997**, *36*, 15006−15012.
(50) Alies, B.; Pradines., V.; Llorens-Alliot., I.; Sayen., S.; Guillon., E.; Hureau., C.; Faller., P. Zinc(II) Modulates Specifically Amyloid Formation and Structure in Model Peptides. *J. Biol. Inorg. Chem.* **2011**, *16*, 333−340.
(51) Khurana, R.; Coleman, C.; Ionescu-Zanetti, C.; Carter, S. A.; Krishna, V.; Grover, R. K.; Roy, R.; Singh, S. Mechanism of Thioflavin T Binding to Amyloid Fibrils. *J. Struct. Biol.* **2005**, *151*, 229−238.
(52) Hudson, S. A.; Ecroyd, H.; Kee, T. W.; Carver, J. A. The Thioflavin T Fluorescence Assay for Amyloid Fibril Detection Can be Biased by the Presence of Exogenous Compounds. *FEBS J.* **2009**, *276*, 5960−5972.